# Inverting raypath-dependent delay times to compute S-wave velocities in the near-surface

Raul Cova and Kris Innanen

## ABSTRACT

Characterizing the near-surface is an important part of solving seismic static problems. It is also a critical step as input for more general iterative inversion methods applied to land seismic data. In the case of converted waves this becomes even more true due to the large magnitudes of the shear-wave statics. Here we propose two solutions based on the inversion of traveltimes in the near-surface. First we address the problem of the parameterization of the inversion. Results show that performing the inversion in the rayparameter domain removes the ambiguities that exist in the raypath-angle domain. The first model we invert is based on transmission traveltimes solely in the low velocity zone. This applies to the inversion of uphole data, but introduces the requirement that multiple offsets be recorded. Secondly, a solution based on the difference in reflection traveltimes between receivers is proposed. This solution may be useful for inverting traveltimes retrieved by interferometric techniques. Due to the complexity of the partial derivatives of the forward modelling operator for this case we decided against local descent-based methods, adopting instead a simulated annealing inversion method. This is also justified by the complex topography of the objective function. Performing a representative number of iterations of the proposed algorithm successfully retrieves the true parameters of the model. Since traveltime differences were used, the inverted parameters only allowed us to compute changes in the depth of the base of the near-surface rather than its absolute value. This can be fixed through a calibration process given the depth of the low velocity zone for at least at one receiver location. Near term plans include extending the results to the full 2D problem and testing on the CREWES 2014 Priddis data set.

## INTRODUCTION

Computing shear wave velocity models for the near-surface is one of the most difficult tasks in the processing of converted wave data. One of the reasons for this is that multicomponent seismic data are usually acquired using P-wave sources. This prevents us from using S-wave critical refractions, as is usually done in the processing of vertical-component data. Since the early 80's the inversion of ground roll dispersion, using techniques like the multi-spectral analysis of surface waves (MASW), has proven to be a useful tool for computing S-wave statics (Mari, 1984; Wattrus, 1989; Park et al., 1999). However, the MASW approach may lack sufficient resolution when strong lateral variations of S-wave velocities are present (Lin and Lin, 2007) or when the near-surface is not horizontally layered (Bodet et al., 2005).

More recently, a technique based in interferometric principles has been developed for redatuming applications. Henley (2012) introduced a raypath-consistent method for solving S-wave statics using an interferometric approach. In this method delay times caused by the near-surface are retrieved by cross-correlating reflection amplitudes in the radial trace domain. Since it is a reflection based method there is no need for the analysis of S-wave

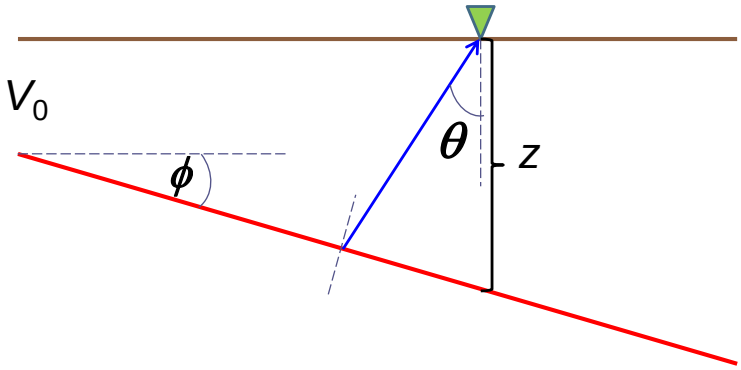


FIG. 1. Basic geometry used for computing traveltimes from a dipping interface to a fixed receiver location at different raypath angles.

refractions. Moreover, Cova et al. (2013) showed how the cross-correlation functions retrieved during this processing exhibit variations that follow the changes in the structure of the near-surface.

In this work we show how raypath-dependent traveltimes can be used to invert a velocity model for the near-surface. We first address the issue of the parameterization of the problem assuming that traveltimes in the near-surface layer are known. In this case we will use a quasi-Newton nonlinear inversion to solve for the parameters of the model. Secondly, we propose a reflection-based solution where the difference in traveltimes due to the near-surface between two receivers is used as the input. In this case, the problem becomes highly nonlinear and the derivatives needed for implementing a Newton's inversion become very complicated. Instead, we will show a solution based on a simulated annealing algorithm that will provide us with a solution for this problem.

## INVERSION OF RAYPATH-DEPENDENT TRAVELTIMES

Figure 1 depicts the problem we wish to solve first. Given a set of traveltimes along rays with different raypath angles ($\theta$), we wish to invert for the velocity ($V_0$), thickness ($z$) and the dip ($\phi$) at the base of the low velocity zone. The traveltimes along each ray can be computed using the relationship,

$$t(\theta) = \frac{z}{V_0}\frac{\cos(\phi)}{\cos(\theta-\phi)}. \tag{1}$$

The same equation can be written in terms of the rayparameter ($p$) as,

$$t(p) = \frac{z}{V_0^2(q + p\tan(\phi))}, \tag{2}$$

where $p$, also known as the horizontal slowness, and $q$ the vertical slowness are given by,

$$p = \frac{\sin(\theta)}{V_0}, \tag{3}$$

$$q = \frac{\cos(\theta)}{V_0}. \tag{4}$$

The vertical slowness can also be written in terms of $p$ as,

$$q = \frac{1}{V_0}\sqrt{1 - V_0^2 p^2}. \tag{5}$$

The events recorded in exploration seismic data arrive at the surface within a range of raypath angles. Thus, the time seismic waves spend in the near-surface varies according to equation 1 or 2. Since, there are three unknowns in these equations and usually more than three raypath angles are recorded, solving for the parameter of the near-surface becomes an overdetermined problem.

**Quasi-Newton nonlinear inversion**

To solve this problem we tried a quasi-Newton inversion approach. In this kind of inversion an initial guess for the model parameters is iteratively updated until the minimum of an objective function is reached. The objective function ($\Phi(\mathrm{m})$) we used here was the $L_2$ norm of the data misfit ($\delta\mathrm{d}$) given by,

$$\Phi(\mathrm{m}) = ||\delta\mathrm{d}||^2 = ||\mathrm{g(m)} - \mathrm{d_{obs}}||^2, \tag{6}$$

where $\mathrm{d_{obs}}$ is the observed data and $\mathrm{g(m)}$ is the forward modelled data for a given set of model parameters $\mathrm{m}$.

In a quasi-Newton approach of the type we apply here, the model parameters are updated as follows:

$$\mathrm{m_i} = \mathrm{m_{i-1}} + \delta\mathrm{m_i}, \tag{7}$$

where the subindex $i$ denotes the iteration number and $\delta\mathrm{m}$, the model update is given by,

$$\delta\mathrm{m} = \left[\mathrm{J(m)}^\dagger \mathrm{J(m)}\right]^{-1} \mathrm{J(m)}^\dagger \delta\mathrm{d}. \tag{8}$$

Here, ($^\dagger$) denotes the transpose operator and $\mathrm{J(m)}$ is the Jacobian or sensitivity matrix, with elements:

$$\mathrm{J(m)} = \left[\frac{\partial \mathrm{g(m)}}{\partial \mathrm{m}}\right]. \tag{9}$$

In our inversion problem there are three parameters we need to solve for ($\phi, V_0, z$). Thus, the terms in the sensitivity matrix are,

$$\mathrm{J(m)} = \left[\frac{\partial \mathrm{g(m)}}{\partial \mathrm{z}}, \quad \frac{\partial \mathrm{g(m)}}{\partial \mathrm{V_0}}, \quad \frac{\partial \mathrm{g(m)}}{\partial \phi}\right]. \tag{10}$$

The form of the derivatives in equation 10 depends on the parameterization chosen for the forward modelling operator. As we show in the next sections this choice can have a significant impact on the character of the inversion.

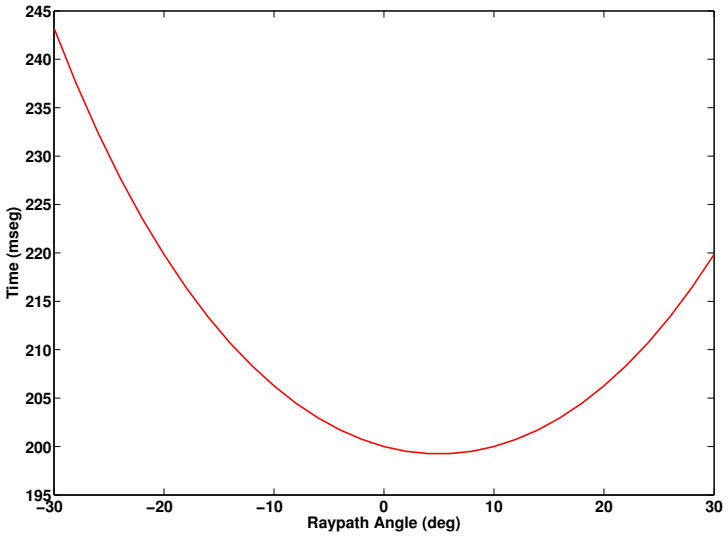


FIG. 2. Modelled traveltimes for a near-surface model with $V_0 = 500$m/s, $z = 100$m and $\phi = 5°$. Notice the shift of the minimum traveltime toward the raypath-angle equal to the dip of the base of the LVL. Also, traveltimes recorded at angles with different sign show several milliseconds of difference.

## Raypath angle parameterization

Using equation 1 as the forward modelling operator of the inversion, the sensitivities in the Jacobian take the following form,

$$\frac{\partial t(\theta)}{\partial z} = \frac{1}{V_0}\frac{\cos(\phi)}{\cos(\theta-\phi)}, \tag{11}$$

$$\frac{\partial t(\theta)}{\partial V_0} = -\frac{z}{V_0^2}\frac{\cos(\phi)}{\cos(\theta-\phi)}, \tag{12}$$

$$\frac{\partial t(\theta)}{\partial \phi} = -\frac{z}{V_0}\frac{\sin(\phi)}{\cos^2(\theta-\phi)}. \tag{13}$$

In order to test this solution synthetic data were created assuming a low velocity layer (LVL) with a thickness of $z = 100$m, velocity, $V_0 = 500$m/s and dip, $\phi = 5°$. Figure 2 shows the traveltimes for this model. There we can see how the traveltime curve is shifted to the right, indicating that the minimum traveltime does not correspond with the vertical traveltime. We can also note that for the same raypath angle value, the traveltime in the near-surface will differ, depending upon the sign of the angle. This means that, in the offset domain, data recorded at positive or negative offsets may experience different static delays regardless of having the same absolute offset value. Finally, if raypath angles of about -20°are reached, the difference relative to the vertical traveltime is about 20ms. Extra delays of this magnitude may degrade the stacking power in a seismic section. All these observations imply that applying a constant trace shift, as in a surface consistent approach, will not be enough to solve the static problem.

Figure 3 shows the inversion results for an initial guess with $z = 50$m, $V_0 = 400$m/s and $\phi = 1°$. There we can see that the inverted parameters are far from the true parameters.

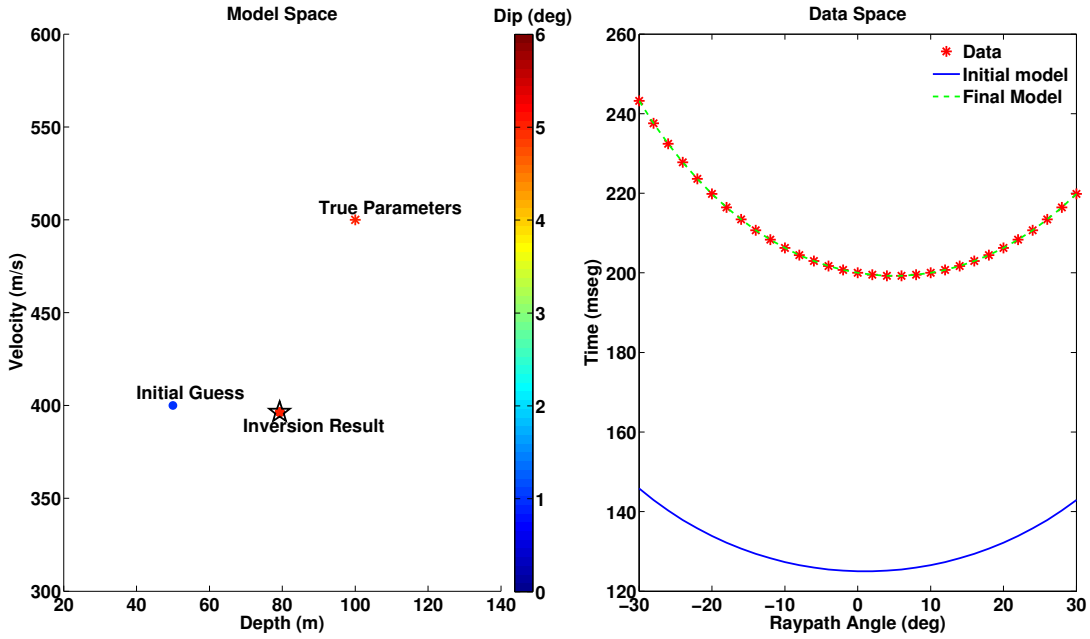


FIG. 3. Inversion results in the raypath angle domain. Although in the data space (right) the modelled data matches the observed data, in the model space (left) the inverted parameters are still far from the true parameters of the model.

However, in the data space we can see that the data modelled with the inverted parameters exactly matches the observed data. This is a result of the non-uniqueness of the problem, in which different model parameters lead to either identical data or data variations that are negligible and/or fall below the ambient noise level. To solve this problem additional regularization terms can be included in the inversion in order to constrain the results.

To better understand the behaviour of the inversion we plotted the objective function for a set of fixed model parameters. Figure 4 shows that the objective function seems to be very well behaved for a fixed thickness or velocity. In both cases the plots show well defined minima at the location of the true parameters of the model. On the other hand, for a fixed dip we can see that there are different combinations of thickness and velocity that provide a minimum of the objective function. For this reason, the inversion was always able to retrieve the true dip but not the velocity and the thickness of the LVL.

In the next section we explain how this response can be improved by simply using a different parameterization in the inversion.

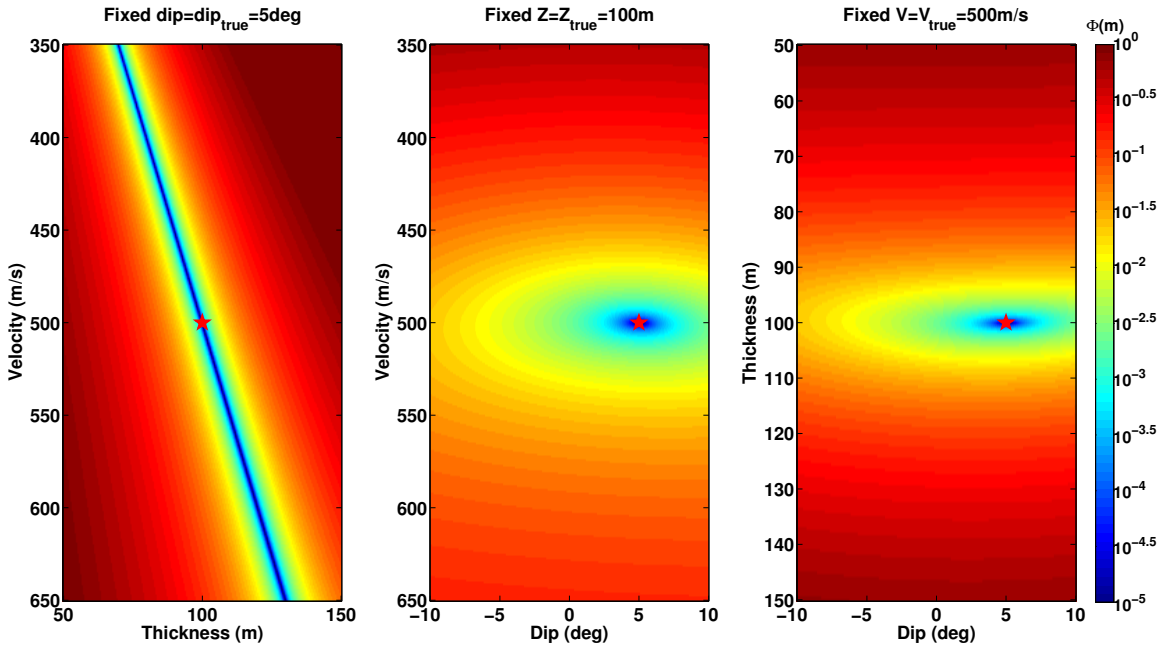


FIG. 4. Objective function map at different fixed model values. Notice that for a fixed velocity and thickness the objective function shows a well defined minimum at the location of the true parameters of the model (red star). However, for a fixed dip, there are multiple combinations of thickness and velocity values that provide a minimum of the objective function.

## Rayparameter parameterization

By using equation 2 as the forward modelling engine of our inversion, the derivatives in the Jacobian matrix become,

$$\frac{\partial t(\theta)}{\partial z} = \frac{1}{V_0^2}\frac{1}{(q + p\tan(\phi))}, \tag{14}$$

$$\frac{\partial t(\theta)}{\partial V_0} = \frac{z}{qV_0^5}\frac{[1 - 2qV_0^2(q + p\tan(\phi))]}{(q + p\tan(\phi))^2}, \tag{15}$$

$$\frac{\partial t(\theta)}{\partial \phi} = \frac{z}{V_0^2\cos(\phi)^2}\frac{1}{(q + p\tan(\phi))}, \tag{16}$$

In this case the derivatives show a more complex form. This is noticeable for the derivative respect to the velocity, where the dependence of $q$ on the velocity introduces additional complexity into the sensitivity.

Figure 5 shows the inversion result using the rayparameter parameterization. In this case we can see the progress of the estimation after each iteration. Notice that the initial parameters used to start the inversion are the same as the ones used in the raypath angle parameterization. However, in contrast to the previous inversion, under the new parameterization the algorithm was able to retrieve the true parameters of the model. In this case not just the modelled data matches the observed data but the retrieved parameters match the true parameters of the model.

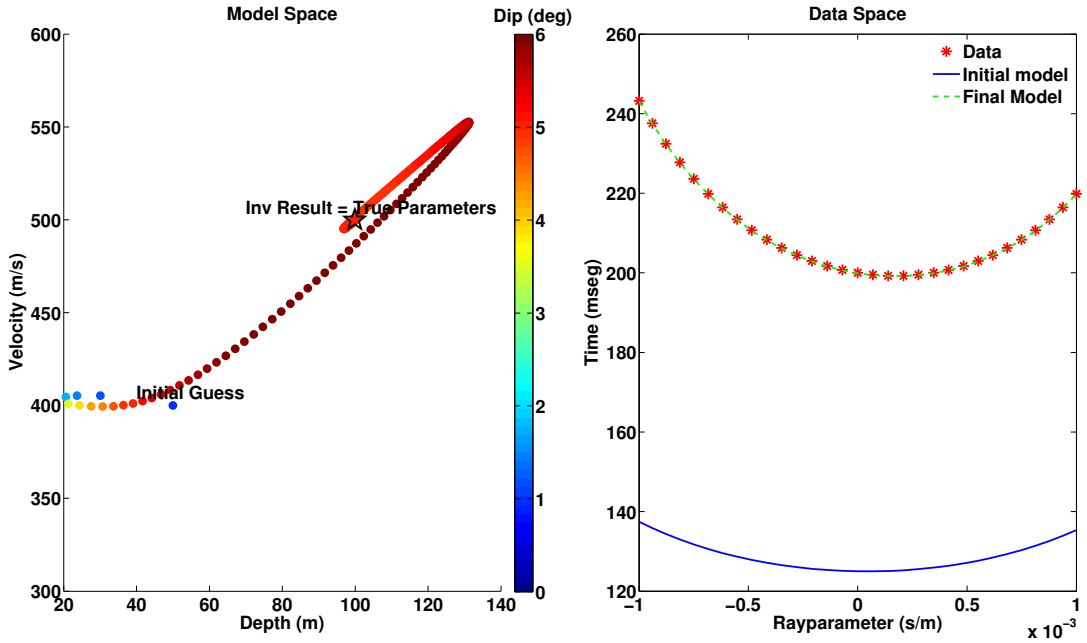


FIG. 5. Inversion results after parameterizing the problem in the rayparameter domain. The scatter points show the progression of the model updates after each iteration. In this case the inversion result (black star) ended up at the exact location of the true parameters.

The reason for this behaviour can be understood by examining figure 6. The plots for the objective function show that for a fixed dip there is just one pair of velocity and thickness values that minimize the objective function. In other words the minimum of the objective function is now constrained around the true parameter values.

Figure 7 shows a comparison between data using two different models in both domains. For the model 1 we used the same parameters we used in the previous tests and for the model 2 we used $z = 70$m, $V_0 = 450$m/s and $\phi = 5°$. As we can see in the plots, the traveltimes given by both models exactly match each other in the raypath-angle domain. However, in the rayparameter domain they show very different traveltimes. Thus, the rayparameter parameterization helps in the solution of the non-uniqueness of the inversion result. The dependence of $p$ on the velocity of the near-surface helps to constrain the inversion performance. Since $p$ is a parameter we can compute from our data, it makes it a good candidate for parameterizing our inversion problems.

## INVERSION OF TRAVELTIME DIFFERENCES BETWEEN RECEIVER LOCATIONS

To use the previous solution we would need to perform a seismic experiment with sources placed at the base of the near-surface. Such acquisition is usually only possible in uphole experiments. However, in conventional uphole surveys a single receiver is deployed on the surface making it impossible to record angle-dependent traveltimes. An alternative is to extend the conventional uphole experiment to one with multiple receivers at different offsets so raypath-dependent properties can be studied.

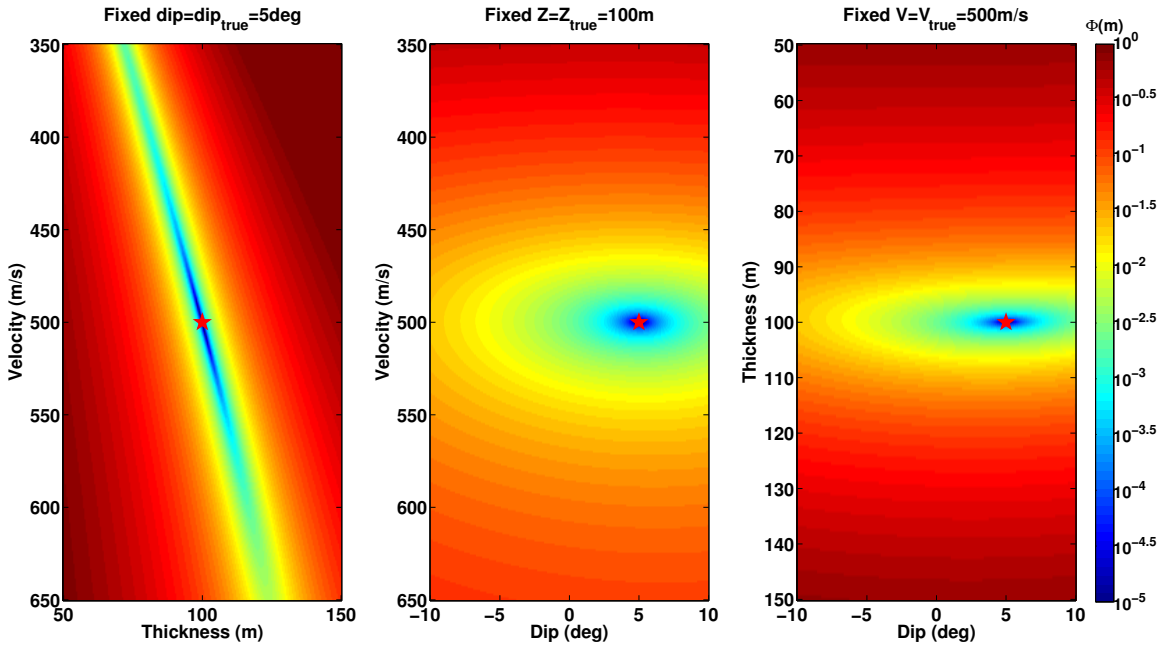


FIG. 6. Objective function map for the parameterization in the rayparameter domain. The minimum of the objective function is now well constrained around the true parameters of the model (red star).

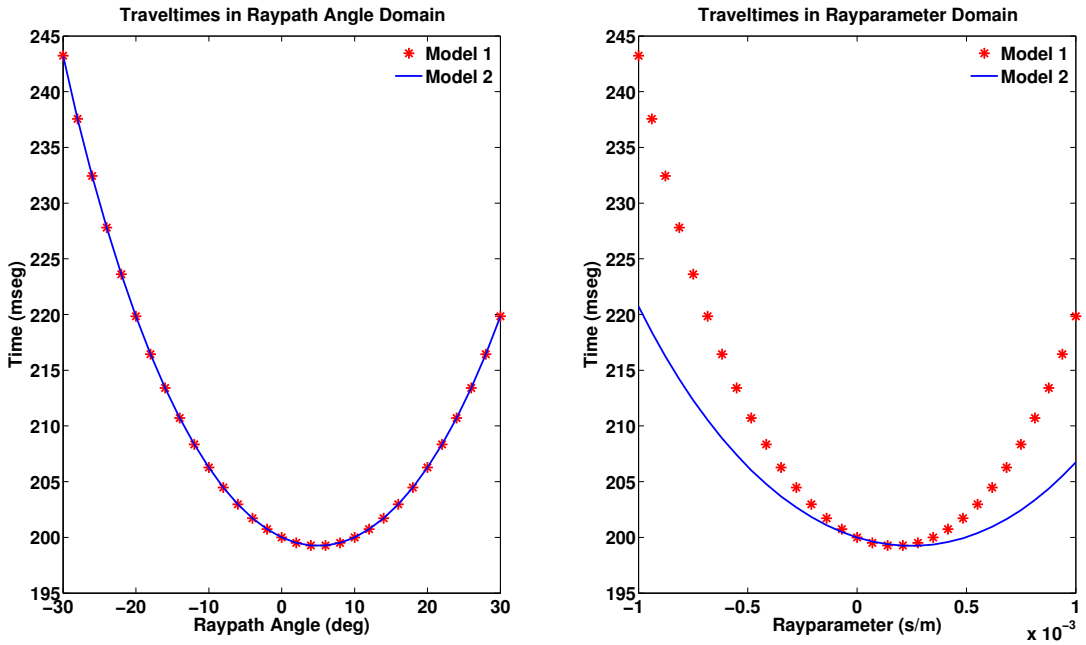


FIG. 7. Data comparison in the raypath angle (left) and rayparameter domain (right). Both model 1 ($z = 100$m, $V_0 = 500$m/s, $\phi = 5°$) and model 2 ($z = 70$m, $V_0 = 450$m/s, $\phi = 5°$) produce the same traveltimes in the raypath angle domain. In the rayparameter domain both models are easily differentiated.

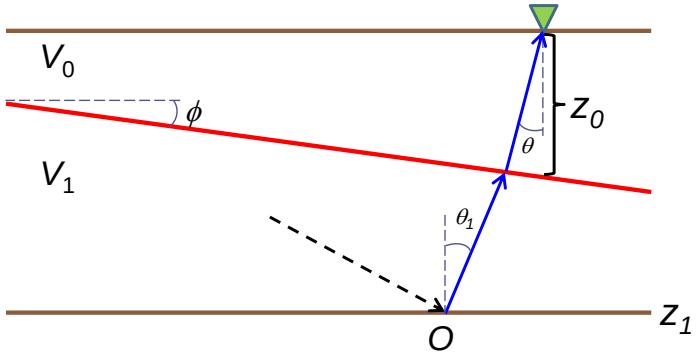


FIG. 8. Model used to compute receiver-side traveltimes from a reflector to a fixed receiver location on the surface.

Here we propose a reflection-based method that uses the difference in arrival times between receiver stations to characterize the near-surface. Figure 8 shows the geometry used for computing the upgoing traveltime recorded at a fixed receiver location in terms of the raypath angles in both media. The model consist of a LVL with a dipping base overlying a medium with a flat base from where reflections are produced. The traveltime for this geometry can be computed as,

$$t(\theta) = \frac{Z_1}{V_1 \cos(\theta_1)} + \frac{Z_0 \cos(\phi)}{V_0 \cos(\theta - \phi)} \left(1 - \frac{V_0 \cos(\theta)}{V_1 \cos(\theta_1)}\right) \tag{17}$$

where $V_1$, $Z_1$ and $\theta_1$, are the velocity, thickness and propagation angle in the underlying medium.

Notice that if there were no dip, and velocities were the same, implying that the propagation angles were also the same, equation 17 reduces to,

$$t(\theta) = \frac{Z_1}{V_1 \cos(\theta_1)} \tag{18}$$

which represent the traveltimes from the reflector to the surface without near-surface effects. Hence, the second term of equation 17 contains the extra delays caused by the presence of a low velocity layer.

To isolate the second term in equation 17 we can subtract traveltimes recorded at two different receiver location and measured with the same raypath angle. If the reference reflector is flat and the velocities are laterally homogeneous, the difference in traveltime between the two receiver locations is a function of the changes in the structure of the low velocity layer. This is also true for a horizontally stratified medium as depicted in figure 9. In this model, for a fixed raypath angle, the traveltime contribution of each layer is the same independent of the receiver location. Since the near-surface is the only layer assumed to have structure, the difference in traveltimes only responds to differences in the structure

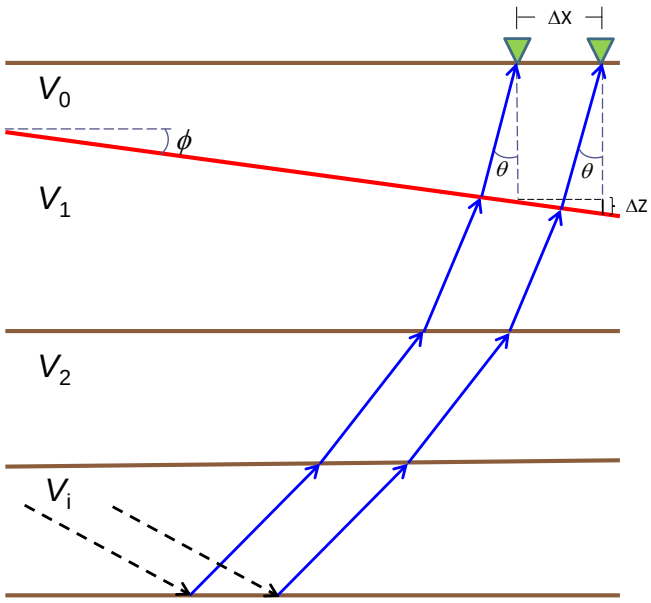


FIG. 9. Extension of the original model to multiple layers. Since strata are assumed to be flat, changes in traveltimes, between receivers locations, are only due to changes in the structure of the near-surface. Notice that the traveltimes must be recorded at the same raypath angle for this assumption to be valid.

of this layer. This traveltime difference can be computed as,

$$\Delta t(\theta) = \frac{\Delta Z_0 \cos(\phi)}{V_0 \cos(\theta - \phi)} \left(1 - \frac{V_0 \cos(\theta)}{V_1 \cos(\theta_1)}\right) \tag{19}$$

$$= \frac{\Delta X \sin(\phi)}{V_0 \cos(\theta - \phi)} \left(1 - \frac{V_0 \cos(\theta)}{V_1 \cos(\theta_1)}\right) \tag{20}$$

This equation can also be written in terms of vertical and horizontal slownesses as,

$$\Delta t(p) = \frac{\Delta X \tan(\phi)}{V_0^2 (q_0 + p_0 \tan(\phi))} \left(1 - \frac{V_0^2 q_0}{V_1^2 q_1}\right) \tag{21}$$

The main problem with this solution are the terms that depend on $\theta_1$. For a flat near-surface, this angle could be easily computed by using Snell's law directly. However, due to the presence of dip at this interface the rayparameter values are going to differ. The magnitude of this difference depends on the velocity of both media and the dip of the interface, as is shown on equation 22.

$$\cos(\theta_1) = \left[1 - (V_1 P)^2\right]^{1/2} \cos(\phi) - P \sin(\phi) \tag{22}$$

where,

$$P = p_0 \cos(\phi) - q_0 \sin(\phi) \tag{23}$$

The dependence of $\theta_1$ on the model parameters makes the inversion problem highly nonlinear. Moreover, the partial derivatives of equation 21 are very complex due to the

trigonometric functions and division operations involved. In order to perform an inversion under these conditions we moved to a non descent-based method, in this case a global optimization strategy using simulated annealing.

**Simulated annealing inversion**

Simulated annealing is a numerical method that uses an analogy between the physical annealing of metals and the mathematical problem of finding the global minimum of a function (Kirkpatrick et al., 1983). In the physical annealing process a metal is heated until it melts and then is cooled very slowly. At high temperatures atomic motions are dominated by random thermal fluctuations. As the temperatures cool atoms begin to develop an orderly minimum-energy crystal.

In the inversion algorithm a function $\mathrm{T}$ is defined as the analog of the temperature. In this study we adopt a quadratic decay as shown in equation 24,

$$\mathrm{T_i} = k\Phi(\mathrm{m_0}) \left( \frac{\mathrm{N} - \mathrm{i}}{\mathrm{N}} \right)^2 \tag{24}$$

where, $k$ is a constant related to how much initial heat is given to the system, $\mathrm{i}$ is the iteration index and $\mathrm{N}$ is the total number of iterations. Under this approach, the objective function ($\Phi(\mathrm{m})$) is now a measure of the energy of the system. Thus, the goal is to find the model parameters that provide the state of minimum energy (global minimum) in the system.

The algorithm begins with an initial guess of the model parameters $\mathrm{m_0}$. A trial solution is then generated by adding an increment ($\Delta\mathrm{m}$) to the initial guess. This increment is randomly drawn from a Gaussian distribution centred around the initial guess. Then, the objective function with the new model parameters ($\Phi(\mathrm{m_{i+1}})$) is compared against the value for the initial guess. The new parameters will be always accepted if the new value of the objective function is lower that in the previous iteration ($\Phi(\mathrm{m_{i+1}}) \leq \Phi(\mathrm{m_i})$). However, to simulate the random atomic motion of the physical annealing process, sometimes model parameters where $\Phi(\mathrm{m_{i+1}}) > \Phi(\mathrm{m_i})$ can also be accepted. To decide this case a test parameter $\mathrm{A}$ (equation 25) is computed and compared to a random number $r$ drawn from an uniform distribution between 0 and 1. If $A > r$ the new solution is accepted even though the value of the objective is higher than in the previous iteration.

$$A = \exp\left( -\frac{\Phi(m_{i+1}) - \Phi(m_i)}{T} \right) \tag{25}$$

When the temperature values are high, the test parameter $A$ is always close to one and solutions are almost always accepted, regardless of the value of the objective function. This feature allows the method to sample a broad region of the model space that may include the global minimum and, possibly, some local minima. As $\mathrm{T}$ decreases the $A$ values will tend to zero, forcing the algorithm to accept only those solutions that minimize the objective function, leading the inversion toward the global minimum of the function.

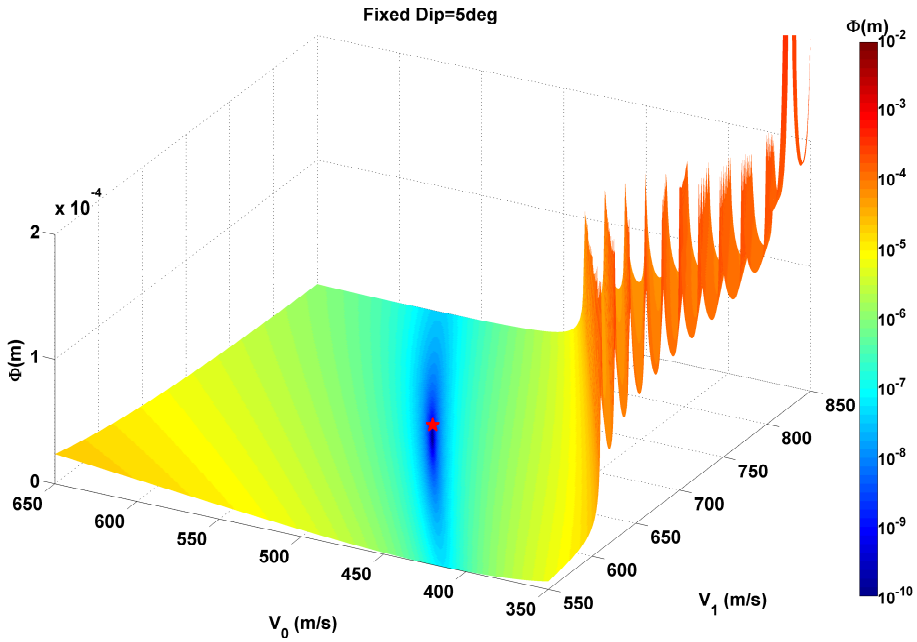


FIG. 10. Two-media model objective function for a fixed dip value. Notice the presence of a series of local minima in the areas coloured in orange.

## Inversion of traveltimes using simulated annealing

Figures 10 to 12 show three plots of the objective function for the inversion of equation 21. The objective function now displays a very complex topography. There we can see, in orange, different series of local minima that may be a challenge for a gradient-based inversion method.

Due to the complex topography of the of the objective function and the partial derivatives of equation 21, we discarded using a quasi-Newton approach. Instead, we adopted the simulated annealing method described in the previous section.

Figure 13 shows one realization of the simulated annealing inversion. There we can see the progressive decay of the temperature and the objective function. It is important to note that for the first half of the iterations the objective function displays a high variability. This is the part of the algorithm where trial solutions are accepted even if they lead to higher objective function values. In the bottom three panels we can also see how the parameter values used in every iteration also show a high variability. This is evidence of how the randomness that dominates the code at high temperatures allows it to explore a wide area of the model space.

In the second half of the iterations shown in figure 13, the objective function variability decreases. At the last thousand iterations, only trial parameters that lead toward a lower value of the objective function are accepted. In the model parameter plots we can see how those trial values begin to converge toward the actual model parameter values.

The downside of this method is the fact that it may provide different solutions for each realization. To avoid this problem one of the options is to perform several realizations and

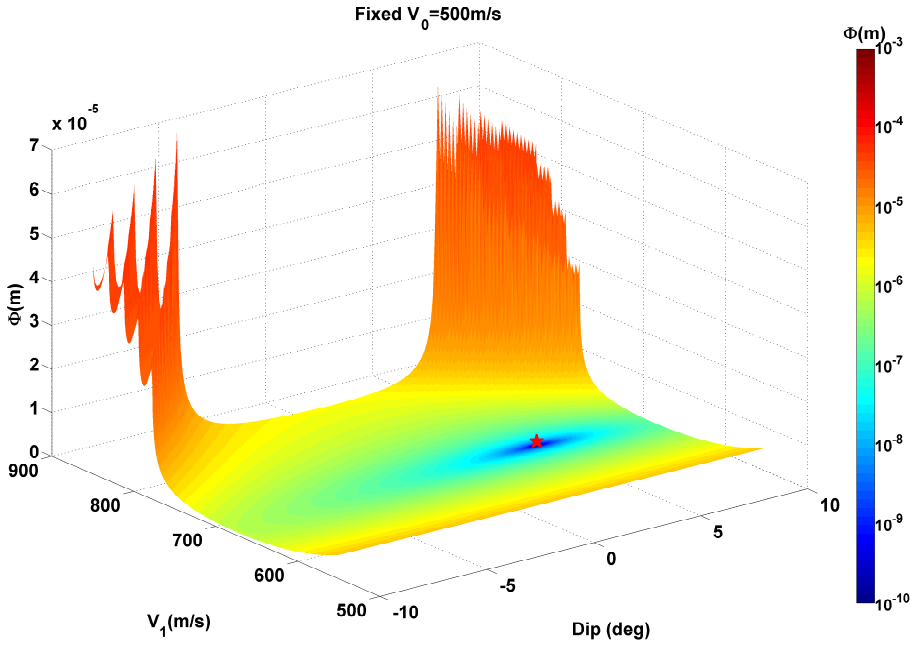


FIG. 11. Two-media model objective function for a fixed $V_0$ value. Notice the presence of a series of local minima in the areas coloured in orange.

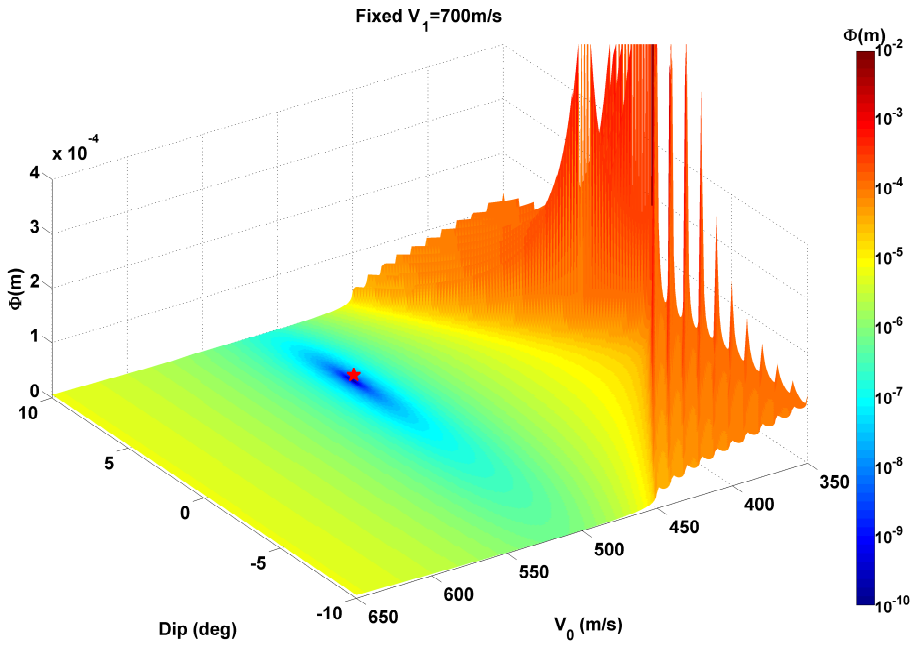


FIG. 12. Two-media model objective function for a fixed $V_1$ value. Local minima can be found in the areas coloured in orange.

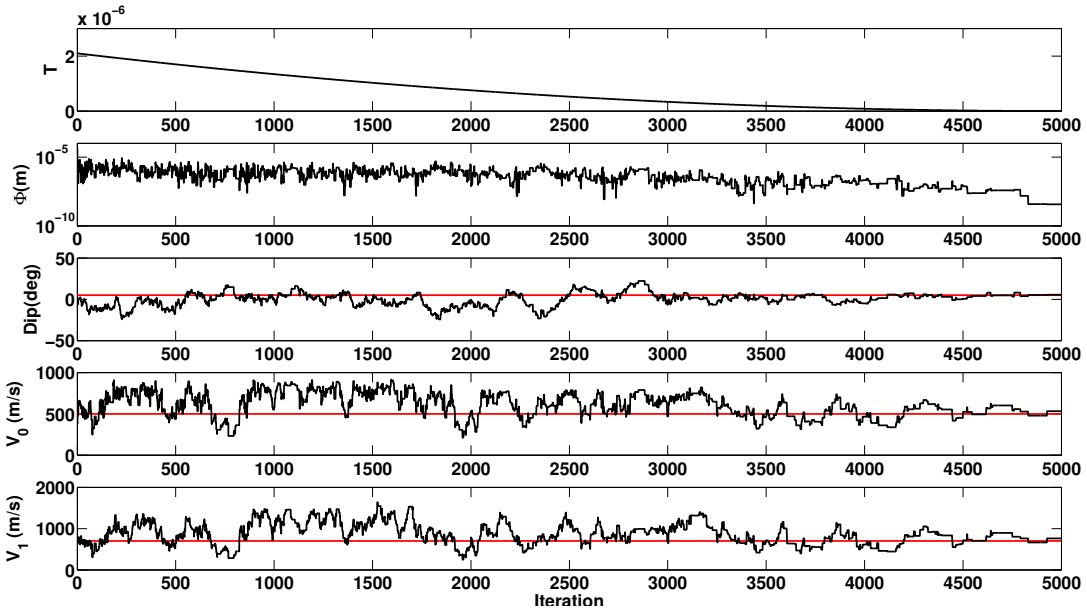


FIG. 13. Evolution of the parameters involved in a simulated annealing realization. Note how the objective function $\Phi(\mathrm{m})$ shows an overall decrease while the trial parameters converge toward the true values of the model (red lines).

then use a statistical metric to retrieve the best solution. Figure 14 shows a histogram of the results for one hundred realizations. There we can see that the distributions are centred around the actual model parameter. In this case, we chose the median of the distribution as the best value for the estimation due to its robustness against outliers. The results show that the inverted parameters are very close to the actual solution.

## CONCLUSIONS

The inversion of near-surface traveltimes in the rayparameter domain proved to be effective in constraining the inversion results. The ambiguity of different thickness/velocity pairs with the same traveltime, for a fixed dip, was clearly resolved in this domain. Since the derivatives of the forward modelling operator were easy to compute the inversion problem was successfully solved using a quasi-Newton non-linear inversion.

When dealing with reflection data additional parameters come into play in the problem of characterizing the near-surface. The method proposed in this study uses the differences in traveltimes between receivers in order to retrieve the changes in the structure of the near-surface. The complex topography of the objective function for this problem and the complexity of the partial derivatives in the Jacobian, led us toward a non-gradient based inversion method. The simulated annealing algorithm used here, proved to be effective in recovering the true parameters of the model.

Traveltime differences can be retrieved by using interferometric principles. Thus, by using cross correlations between receiver gathers in the rayparameter domain, we should be able to characterize the near-surface. Further analysis using synthetic and real seismic data is needed to confirm this idea.

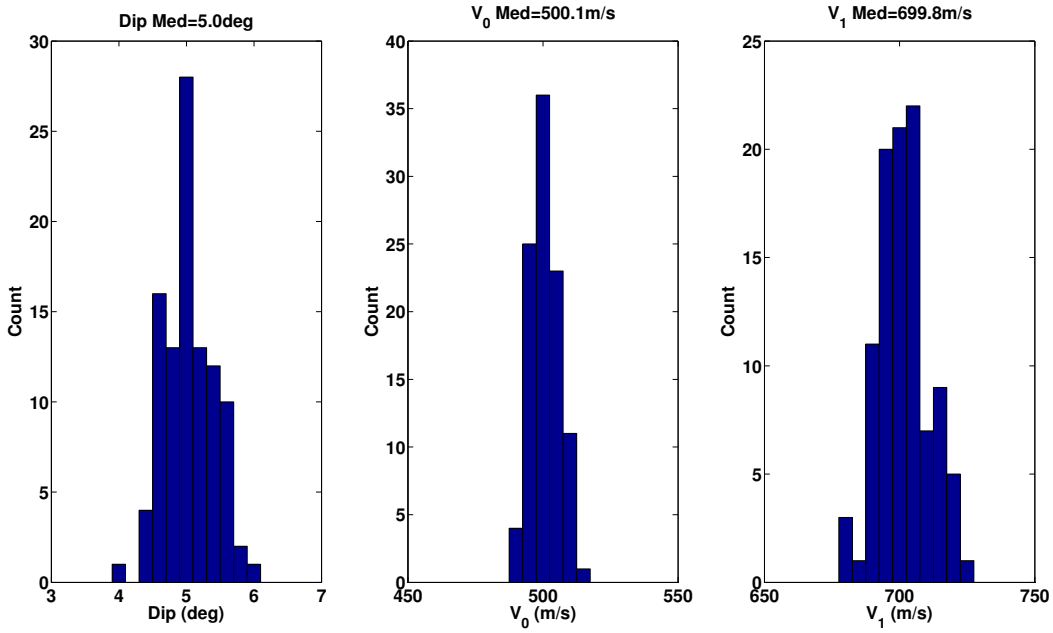


FIG. 14. Distribution of the results given by the simulated annealing inversion after one hundred realizations.

## ACKNOWLEDGEMENTS

The authors would like to thank David Henley for helping in the editing of this report. We also acknowledge CREWES sponsors and NSERC (Natural Science and Engineering Research Council of Canada) for providing the financial support for this research.

## REFERENCES

Bodet, L., van Wijk, K., Bitri, A., Abraham, O., Côte, P., Grandjean, G., and Leparoux, D., 2005, Surface-wave Inversion Limitations from Laser-Doppler Physical Modeling: Journal of Environmental & Engineering Geophysics, **10**, No. 2, 151–162.

Cova, R., Henley, D., and Innanen, K., 2013, Non-stationary shear wave statics in the radial trace domain: CREWES Research Report, **25**, 1–14.

Henley, D., 2012, Interferometric application of static corrections: Geophysics, **77**, No. 1, Q1–Q13.

Kirkpatrick, S., Gelatt, C. D., and Vecchi, M. P., 1983, Optimization by simulated annealing: Science, **220**, No. 4598, 671–680.

Lin, C.-P., and Lin, C.-H., 2007, Effect of lateral heterogeneity on surface wave testing: Numerical simulations and a countermeasure: Soil Dynamics and Earthquake Engineering, **27**, No. 6, 541 – 552.

Mari, J. L., 1984, Estimation of static corrections for shear-wave profiling using the dispersion properties of Love waves: Geophysics, **49**, No. 8, 1169–1179.

Park, C. B., Miller, R. D., and Xia, J., 1999, Multichannel analysis of surface waves: Geophysics, **64**, 800–808.

Wattrus, N. J., 1989, Inversion of ground roll dispersion for near-surface shear-wave velocity variations: 59th Ann. Internat. Mtg., Soc. Expl. Geophys., Expanded Abstracts,, 946–948.